



Electron Structure And Thermodynamics Of Solid Solutions In Ni-H System

^aDr. T. S. Jayanthi, ^{a*}Dr. L. Leena Hebsibai, ^bDr. S. R. Chitra

^aHead and Associate Professor, Department of Physics, Vivekananda College, Agasteeswaram, (Affiliated to Manonmaniam Sundaranar University, Tirunelveli), Tamilnadu, India.

^{a*}Guest Lecturer, Raja Doraisingam Government Arts College, Sivagangai, Tamilnadu, India.

^bHead and Associate Professor, Department of Physics, P K N Arts and Science College, Thirumangalam, Madurai, Tamilnadu, India.

Abstract

The widespread concept of nickel hydride in the Ni-H system is discussed based on the first-principle atomic calculations and experimental X-ray diffraction data. The total cohesion energy in Ni-H solid solution has been determined using the density functional theory and program package Wien2k. Its dependence on hydrogen concentration is shown to be linear, which suggests the absence of any energy barrier for precipitation reaction. Moreover, the second derivative of the calculated solution enthalpy is negative within the hydrogen-to-nickel ratios, H/Ni, of 0.03 to 0.75, which is a sign of spinodal decomposition. These hydrogen concentrations are consistent with the measurements of X-ray diffraction, of which results are usually interpreted in terms of Ni hydride. The density of electron states has been calculated, and its non-monotonous concentration dependence correlates with that of solution enthalpy, as also expected for spinodal decomposition. The obtained results are interpreted as miscibility gap in the Ni-H system with spinodal decomposition having the electron origin. Finally, the “hydrides” in d-metals are discussed in terms of two Gibb’s types of precipitation reactions.

Keywords Nickel; Hydrogen; Ab initio calculations; Spinodal decomposition; Hydride

Introduction

Nickel hydride is the object of studies starting from its discovery in 1958, e.g. [1, 2]. A conclusion about hydride formation in the hydrogen-saturated layer under the surface of the nickel electrode was based on the non-diffusional character of hydrogen desorption kinetics after interruption of the electrochemical charging. Using X-ray diffraction [3, 4], it was shown that this new phase succeeds to the fcc structure of the parent nickel, but with the increased lattice parameter by about 6%. Recently [5], the history of nickel hydride

discovery was stated on the occasion of its 45 years and a stimulating effect of these pioneer works on the studies of metal–hydrogen systems has been briefly described.

Since 1958, a number of experiments were devoted to Ni-H system and the obtained results have created a considerable base for discussion. E.g., measurements of hydrogen penetration in nickel were carried out using the electrochemical technique [6], and three different regions have been distinguished in the potential-composition curves. These regions were interpreted as corresponding to so-called α -phase existing up to the hydrogen-to-metal ratio H/Ni of about 0.03, β -phase with H/Ni of about 0.6 and the region of two phase mixture. Respectively, they were attributed to the hydrogen-depleted Ni-H solid solution, the hydrogen-rich nickel hydride and intermediate zone of transition from the first phase to the second one. Among numerous XRD studies distinguished are the *in situ* experiments during cathodic hydrogen charging, e.g. [7]. The authors recognized two “nickel hydride phases”: α -NiH with low H/Ni ratio (≤ 0.03) and β -NiH_x with $0.6 \leq x \leq 0.7$. Some variation has been found in the stoichiometric coefficient x and ascribed to formation of “the hydrogen ordinary solid solution” on the base of nickel hydride. Other possible interpretations were not analyzed.

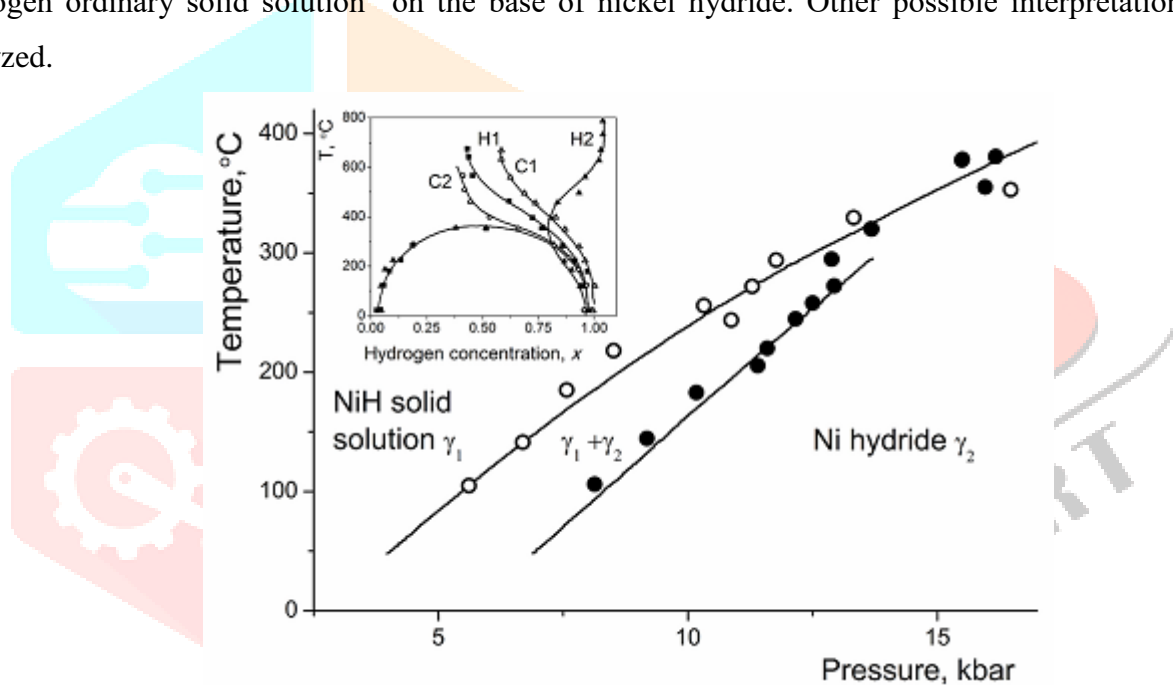


Figure 1 T-P phase diagram Ni-H constructed using high gaseous hydrogen pressures and measurements of electroresistivity, according to [10, 11]. In the insert, the same diagram was obtained using *in situ* X-ray of synchrotron radiation and diffraction measurements at different temperatures and high hydrogen pressures [11, 12].

It was also shown in [3, 8] that decomposition of nickel hydride follows a first order kinetics, whereas the opposite result has been obtained in [9], where the non-linear behavior of the desorption rate has been attributed to the effect of microstructure on the mechanism of phase transition. The saturation of nickel with hydrogen under high hydrogen pressures along with the measurements of electroresistivity allowed to build the phase diagram in the broad range of temperatures and concentrations [10, 11]. Like it was the case for electrochemical hydrogen saturation, e.g. [6, 7], three T-P areas were designated for hydrogen-depleted, hydrogen-rich and mixed phases, respectively. At the same time, a crown was found in the Ni-H phase diagram obtained in [12, 13] at high hydrogen pressures using X-rays of synchrotron radiation. The

corresponding phase diagrams are presented in Figure 1. The interpretation of experimental data was proposed by the authors of [10-14] in terms of nickel hydride.

However, some intriguing points in these diagrams concern the apparent existence of nickel hydride over the extended hydrogen concentration range, which could be natural for solid solutions and can hardly be imagined for chemical compounds to which class the hydrides belong. The occurrence of the crown is a sign for miscibility gap and not consistent with formation of chemical compounds. And the following curious question can be addressed to the both diagrams in Figure 1. What a phase is stable at temperatures above 400 °C: γ_1 or γ_2 ?

The primary aim of the presented work was to study thermodynamics of Ni-H system based on the atomistic calculations combined with measurements of X-ray diffraction and discuss the experimental data in terms of two possible precipitation reactions in solid solutions proposed by the father of thermodynamics J. Willard Gibbs.

Along with that, taking into account a number of recently claimed “metal hydrides” be obtained using hydrogen saturation under high pressures and based on the distinctions in thermodynamics of compounds and solid solutions, we are going to discuss a tendency to delete the border between these two classes of phases.

Calculations and Experimental

Ab initio calculations of hydrogen effect on the electron structure of nickel were performed within the framework of Density Functional Theory (DFT) [14, 15] using the Wien2k program package [16]. According to this theory, the total energy of a studied system, E_{tot} , is presented as a sum of the kinetic energy between non-interacting particles, electron-electron repulsion energy, nuclear-electron attraction energy, an exchange-correlation term and Coulomb repulsive energy of the fixed nuclei.

For the accurate description of the exchange and correlation effects, the Generalized Gradient Approximation (GGA) [17] was used. The convergence tests were performed to find optimal values of wave functions in the basis set and the number of k-points which are used for Brillouin zone sampling according to the Monkhorst-Pack scheme [18]. The wave functions in the unit cell are the spherical ones for the region inside atomic spheres, i.e. ion cores, and the plane waves for the interstitial regions. Such approach gives a necessary flexibility for the basis set, which results in a quicker convergence during the calculations in comparison with the single-type basis and in the better description of the core states.

The unit cell for calculations consisted of 32 nickel atoms with variable quantity of hydrogen atoms to cover a wide range of hydrogen concentrations. In all cases, the spin polarization effects were also included to take into account the magnetic contribution to the total energy. Brillouin zone integration was constructed with the $15 \times 15 \times 15$ k-point mesh. For proper comparison, the muffin-tin radii of nickel and hydrogen atoms, $R_{\text{mt}}(\text{Ni}) = 2.08$ Bohr and $R_{\text{mt}}(\text{H}) = 1.12$ Bohr, were kept constant in the calculations of different atomic configurations. The magnitude of the largest vector G in the Fourier expansion was equal to 20. For accurate determination of atomic positions, the force convergence was set to be 0.1 mRy/a.u. with the interatomic forces between the atoms smaller than 2 mRy/a.u. To find the equilibrium lattice constants, the

Murnaghan's equation of state from Ref. [19] was used by fitting the total energy versus the unit cell volume.

To determine the solution enthalpy of hydrogen atoms in the nickel lattice, the following equation was used:

$$\Delta H_s = E_{tot}(NiH_n) - E_{tot}(Ni) - n/2E_{H_2}, \quad (1)$$

where E_{tot} are total energies of corresponding cells after all types of relaxation (volume, shape, atomic positions) and E_{H_2} is a total energy of the hydrogen molecule, which is calculated by putting two hydrogen atoms in a cubic box with quite large length (20 Bohr) to exclude any possible interactions which can arise because of periodic boundary conditions. Such calculations result in the bond length distance of 0.751 Å, binding energy of 4.70 eV and vibrational frequency of 4270 cm⁻¹, which is in a good consistency with the available experimental values of 0.741 Å, 4.75 eV and 4395 cm⁻¹ [20].

The phonon effects and thermodynamic functions were calculated using Phonon software [21, 22] within the harmonic approximation. To include the effects concerned with phonons, the dynamical matrix has to be constructed. The elements of such matrix are the force constants that could be obtained from *ab initio* calculations according to the direct method [23, 24] and its modification [22]. Afterwards, by constructing the phonon density of states, thermodynamic functions could be determined. Using such approach, the zero-point energy corrections for the systems with hydrogen atoms should be taken into account. In a simplest approximation, the force constants concerned with the displacements of nickel atoms from their equilibrium positions can be equal to zero because the mass of the nickel atom is significantly larger than that of the hydrogen atom. After diagonalization of the Hessian matrix, the normal mode frequencies of hydrogen atoms can be obtained and the zero-point energy can be calculated by summing up the zero-point vibrational energies $E_{zpe} = 1/2 \sum (h \nu_i)$ where ν_i is a real normal mode frequency.

X-ray diffraction has been used to estimate a change in the lattice parameters caused by hydrogen dissolution in the nickel. A pure nickel plate of 0.5 mm in thickness was saturated with hydrogen at room temperature in the aerated 1N H₂SO₄ solution containing 0.01 g/l NaAsO₂ with the current density of 50 mA/cm² for 72 hours. A platinum foil served as the anode. After cathodic charging, the specimens were put into liquid nitrogen to prevent hydrogen degassing. Specimen was installed into the holder of X-ray diffractometer for time less than 120 s.

X-ray diffraction measurements were carried out in Co K_α radiation using Huber diffractometer with one-circle Θ -2 Θ goniometer and operating voltage of 30 kV. A computer program controlled the angular movement of both goniometer and counter. A cryosystem LN-3 produced by Cryo Industries of America Inc. was used for measurements at low temperatures. In contrast to standard cryostats, this system allows the rapid cooling of the sample by the liquid nitrogen flow and measurements at any temperature within the range of +90 °C to -196 °C. Measurements were carried out at -155 °C. For hydrogen degassing, the sample in the diffractometer holder was heated to RT or higher temperatures, held at this temperature for 10 to 15 min and cooled again down to -155 °C for further measurements.

Results

• Ab initio calculations

The comparison of possible positions for hydrogen atoms in the nickel lattice in terms of energy reveals that they prefer to occupy octahedral interstitial sites in the fcc lattice within all the range of studied hydrogen concentrations. This result is consistent with a huge array of experimental data obtained by means of X-ray diffraction measurements (e.g. [4, 25]). Figure 2 demonstrates the total cohesion energy of the calculated Ni-H ensemble as a function of hydrogen concentration. The total cohesion energy was defined as a difference between the calculated total energy per ensemble and the sum of the total energies of free atoms included in this ensemble, $E_c = E_{tot} - \sum E_{tot,at}$, where summation is performed over the all included atoms. Thus, the total cohesion energy characterizes the potential energy of all the interatomic bonds in the studied structure and corresponds to thermodynamic stability of the Ni-H system.

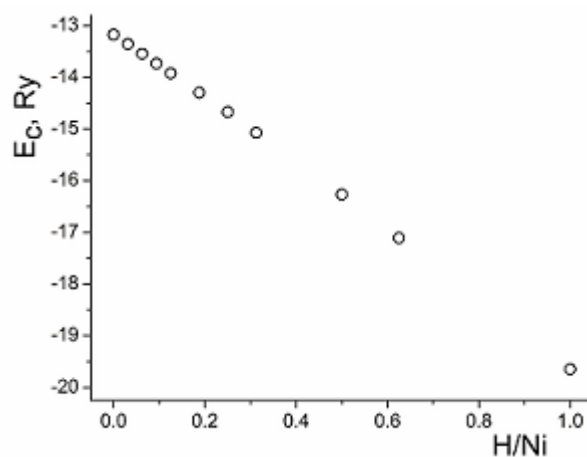


Figure 2 Total cohesion energy as a function of hydrogen concentration in Ni-H system.

As follows from this Figure, the total cohesion energy monotonically decreases with increasing hydrogen concentration in the nickel lattice, which is due to formation of new bonds between the hydrogen and host atoms.

The calculated enthalpy of hydrogen dissolution that includes the zero-point energy correction is presented in Figure 3a. As follows from its concentration dependence, the solution enthalpy increases with increasing H/Ni ratio up to 0.25 and, thereafter, decreases. The second derivative of the solution enthalpy is presented in Figure 3b. As seen, it acquires the negative sign in the concentration range of H/Ni in between 0.03 and 0.75.

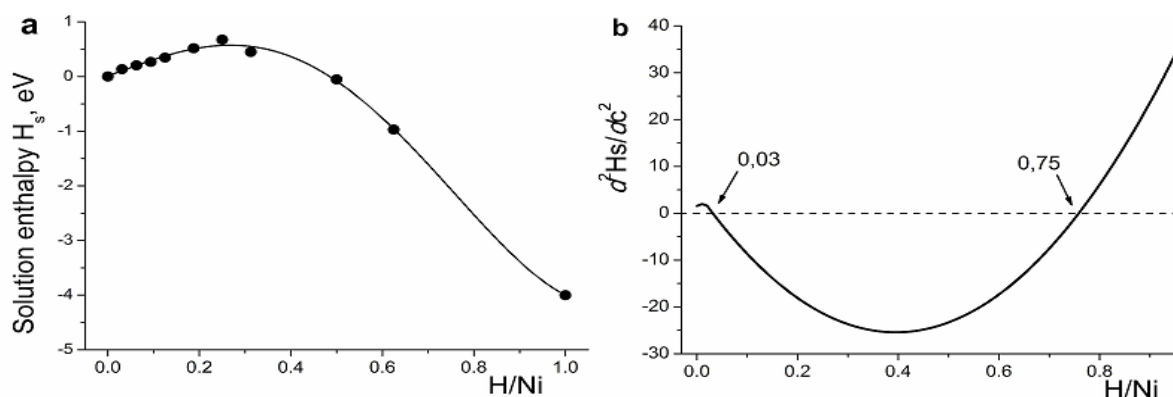


Figure 3 Variation in the hydrogen solution enthalpy for Ni-H system with increasing hydrogen content (a).

Second derivative of the solution enthalpy as a function of hydrogen content (b).

According to the obtained results, the solution enthalpy of one hydrogen atom in the nickel lattice amounts to 0.14 eV, which corresponds to the available experimental data [26-28]. Nevertheless, some remarks should be given here. Usually, measurements of solution enthalpy are being carried out at elevated temperatures and the extrapolation of experimental data to the low temperature range should be done to allow a correct comparison with the data obtained by means of *ab initio* calculations. In [29], the analysis of a large array of experimental data has been carried out and it was shown that the heat of hydrogen solution in nickel tends to be increased with increasing temperature. The calculated total density of states, DOS, for the spin up and spin down electron states in the NiH_x system is shown in Figure 4a and 4b in comparison with that in the pure nickel.

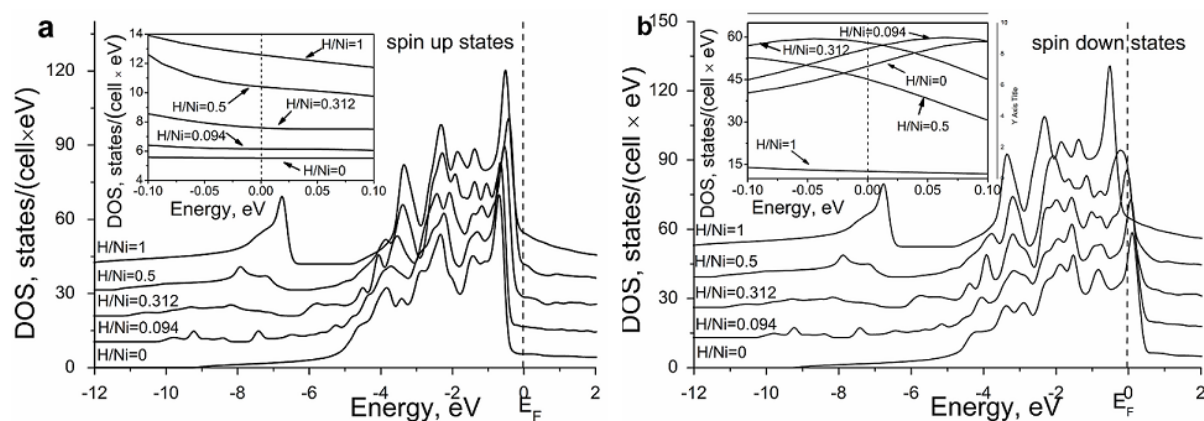


Figure 4 Concentration dependence of density of electron states for spin up (a) and spin down (b) in the Ni-H system in comparison with that in the pure Ni.

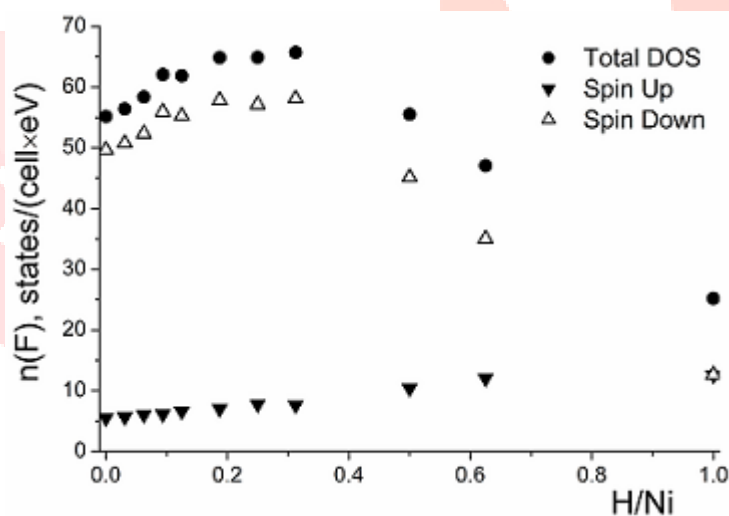


Figure 5 Density of states at the Fermi level as a function of hydrogen concentration for different spin orientations.

A detailed behavior of the DOS in the vicinity of the Fermi level is shown in the insert to each Figure. In case of pure nickel, the bonding and antibonding states for the spin up channel are almost completely filled, whereas for the spin down channel, the antibonding states are only partly filled. The interaction between nickel and hydrogen atoms results in the appearance of bonding states at the bottom of the metallic d-band. The analysis of partial contributions to the total DOS from the electrons of different atoms and different symmetries reveals that the Ni 4s and H 1s electrons are fully overlapping and form the Ni-H bonds. Because of degeneration, the 3d orbital is split into e_g and t_{2g} groups which are different in their symmetry. According to the obtained results, the 3d e_g electrons also contribute to the Ni-H bonds, whereas the 3d t_{2g}

electrons are localized and do not take part in the Ni-H interaction. The effect of hydrogen on the DOS at the Fermi level is remarkable (see the inserts in Figure 4).

With increasing hydrogen content, it increases moderately and monotonously for the majority spin channel (Figure 4a), whereas its behavior is non-monotonous for the minority spin channel (Figure 4b). Corresponding concentration dependences of spin up and spin down electron states and their total values are presented in Figure 5. Up to the H/Ni ratio of about 0.27, the DOS at the Fermi level for the minority channel and the total DOS increase, however, above this hydrogen concentration, they decrease. Such a substantial decrease in the DOS at the Fermi level is caused by the filling of the antibonding states. It explains the magnetic behavior of the H-saturated nickel which becomes paramagnetic at high hydrogen contents according to the experimental data [30].

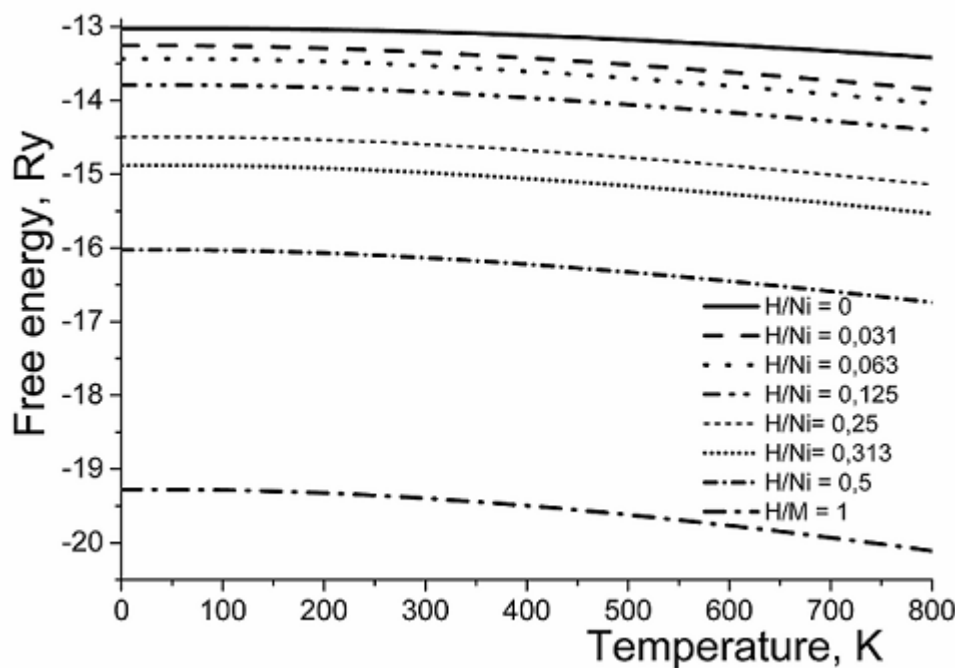


Figure 6 Temperature dependence of Helmholtz free energy for different hydrogen concentrations in Ni-H system.

The phonon contribution was calculated within the frame of harmonic approximation. As follows from the obtained data, see Figure 6, with increasing hydrogen content, it does not change the general behavior of free energy within the studied temperature range. This is an indication that precipitation reaction in the Ni-H solid solutions has the electron nature.

- **X-ray diffraction**

X-ray diffraction patterns measured at $-155\text{ }^{\circ}\text{C}$ after installation of the hydrogen-charged sample into the holder and successive heating procedures are presented in Figure 7. The intensive peak $(111)\gamma_a$ and rather small peak $(111)\gamma_1$ are recorded just after sample installation. Heating at the first and second stages of hydrogen degassing due to holding at 295 K for 10 min, respectively, shift the $(111)\gamma_a$ peak to the position $(111)\gamma_b$ and, then, to γ_2 , whereas intensity of peak $(111)\gamma_1$ increases without a visible change in its position. Further stages of hydrogen degassing due to holding of the sample at RT and higher temperatures result in the exchange of peak intensities between γ_2 and γ_1 , of which positions remain to be stable within the error of measurements.

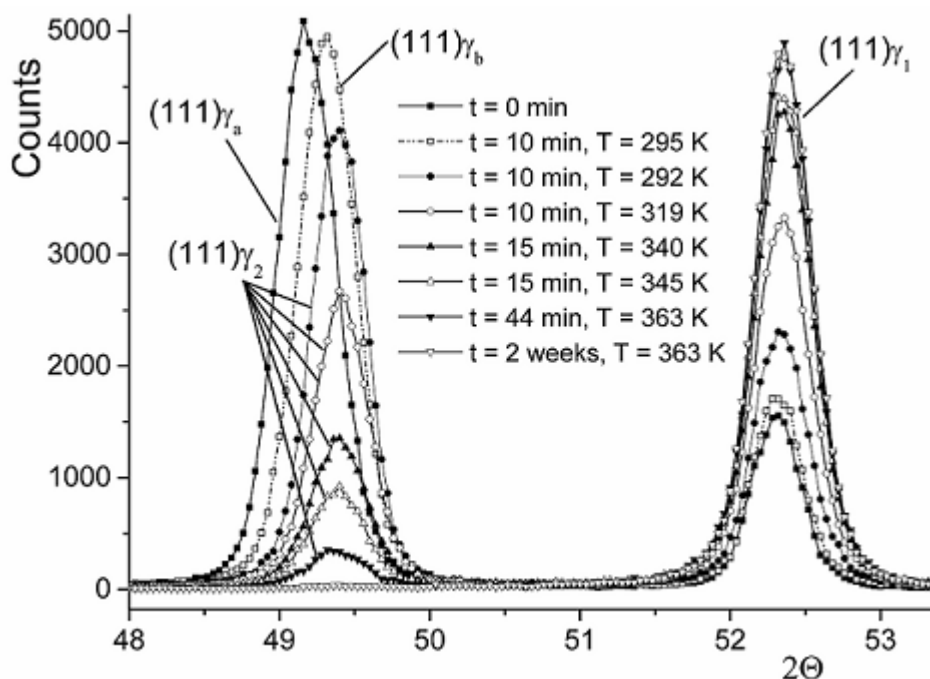


Figure 7 X-ray diffraction in the hydrogen-charged nickel.

Measurements were performed at $-155 \pm 5^\circ\text{C}$ with successive intermediate holdings at higher temperatures for a certain period of time. The obtained lattice parameters are 3.725 \AA , 3.715 \AA , 3.710 \AA and 3.514 \AA for, γ_a , γ_b , γ_2 and γ_1 , respectively. Using the data for hydrogen effect on dilatation of metals with the fcc crystal lattice, as proposed by Baranowski et al. [31], one can estimate the atomic ratio H/Ni as 0.73 for γ_a , 0.69 for γ_b , 0.67 for γ_2 and 0.02 for γ_1 with the accuracy of ± 0.005 . The H/Ni ratio n_{γ_1} , as determined from the presented measurements, is close to the $\text{H/Ni} = 0.03$ obtained in our *ab initio* calculations and consistent with a number of available experimental studies. Finally, the sample was heated up to 90°C for 10 min and thereafter held for two weeks at RT. The peak γ_2 has disappeared, whereas position of peak $(111)\gamma_1$, as measured again at -150°C , was practically not changed.

Discussion

- **Thermodynamical basis for transformations in the Ni-H solid solution.**

According to classical theory of solid solutions and in consistency with J. W. Gibbs, two types of precipitation reactions are possible (see, e.g. [32]). In the first type (Figure 8), the Gibbs energy of a supersaturated solid solution cannot be spontaneously reduced to its minimum at given temperature because the curvature of the free energy versus composition curve is always positive.

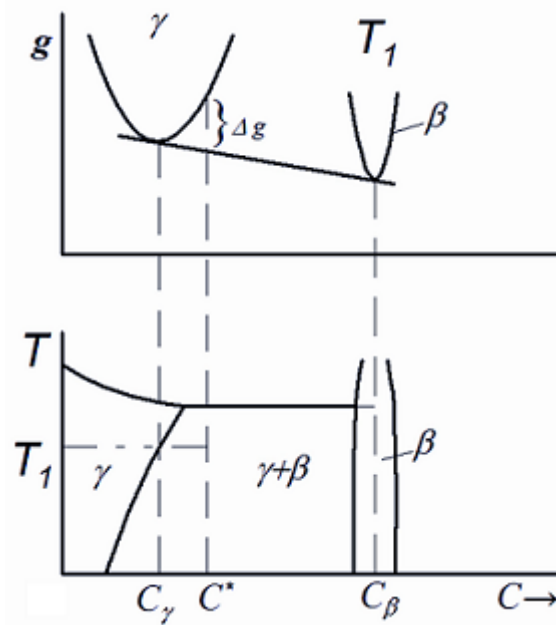


Figure 8 Gibbs energy and corresponding fragments of the phase diagram as function of chemical compositions and temperature for the cases of precipitation of a chemical compound. C_γ - equilibrium concentration, C^* - supersaturation concentration., C_β - concentration in the precipitation phase.

In this case, the Gibbs energy can be decreased only if a new distinctly different phase with lower energy and different crystal lattice is nucleated. This type of precipitation reaction is characterized by some energy barrier which should be overcome to initiate the nucleation process. For example, just this reaction occurs during saturation of the iron with gaseous nitrogen at high pressures resulting in precipitation of the γ' -nitride Fe_4N (see [33]).

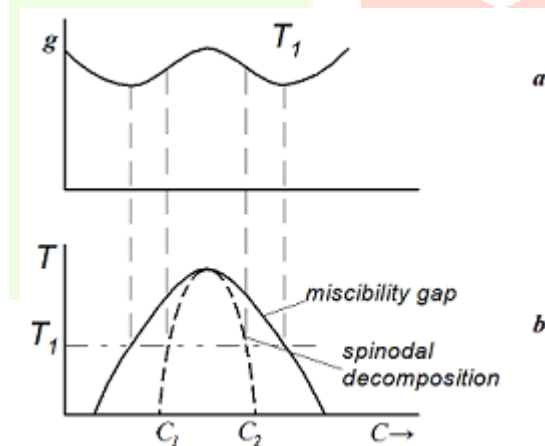


Figure 9 The same, as in Figure 8 for the case of miscibility gap in the supersaturated solid solution.

In the second type of precipitation reactions (see Figure 9), the Gibbs energy is characterized by a single curve with one maximum and two local minima, which is resulted from some positive energy term added to the free Gibbs energy and causing the immiscibility of solid solutions. Phases belonging to this single curve have the same type of the crystal lattice and differ only in the concentration of solute elements. As a result, below some critical temperature denoted as a consolute point, the solid solution is decomposed into two phases of fixed compositions. In the concentration range between the inflection points on the free energy curve, the mechanism of such reaction is the spinodal decomposition.

As follows from the concentration dependence of the total cohesion energy, as presented in Figure 2, it decreases monotonically with increasing hydrogen content in Ni. The absence of any deviations from its linear behavior suggests that the precipitation reaction proceeds without any energy barrier. The absence of energy barrier and the identity of the crystal structures for “nickel hydride” and parent nickel are signs that the dependence of free energy on the hydrogen content should be described by a single curve belonging to both phases, as shown in Figure 9.

Moreover, the non-monotonous behavior of hydrogen solution enthalpy with increasing hydrogen content, as presented in Figure 3a, and its negative second derivative within the H/Ni ratio in between the values of 0.03 and 0.75 are important signs that the precipitation reaction occurs via spinodal decomposition. Within this concentration range, the hydrogen solid solution is decomposed into the hydrogen-rich and hydrogen-depleted phases of fixed compositions on the spinodal reaction.

It is interesting to compare the results of calculations with the experimental data obtained by Baranowski et al. [5], where the electrical resistance of nickel was measured as a function of gaseous hydrogen pressure. A significant change in the electroresistivity was observed if the hydrogen pressure has exceeded 6 kbar, which was attributed by the authors to the formation of the hydride phase. Using the expression for hydrogen concentration, as derived in [34], and taking into account the hydrogen solution enthalpy obtained in our calculations, the H/Ni ratio corresponding to the start of such sudden decrease in the electroresistivity can be estimated as

$$C_H = \alpha \sqrt{F} \exp(-\Delta H/RT) \quad (2)$$

where α is a constant, F is a fugacity, R is the gas constant, ΔH is an enthalpy for dissolution of hydrogen atom in a metal and T is a temperature. The H/Ni ratio of 0.07 is obtained from this estimation. It falls into the above calculated concentration range for the existence of two solid solutions resulted from spinodal decomposition and is close to its low limit.

It was shown earlier that the spinodal decomposition has an electron origin, e.g. [35–38]. Accordingly, a correlation should exist between some parameters describing the electron structure of a system and its inclination to spinodal decomposition. Within the rigid band approximation, the second derivative of the solution enthalpy correlates with the DOS at the Fermi level via the following equation:

$$d^2H/dc^2 \sim 1/n(F) \quad (3)$$

Generally, the rigid band model fails to describe the spinodal decomposition. Nevertheless, the inverse proportionality between solution enthalpy and DOS at Fermi level was confirmed to exist, e.g. [35, 37]. The identical character of the concentration behavior for second derivative of the solution enthalpy, see Figure 3b, with the concentration dependence of the DOS at the Fermi level, see Figure 5, confirms the inverse proportionality between the components of Eq. (3) for the Ni-H system.

- **Comparison with available experimental data.**

The obtained X-ray diffraction data and results of atomistic calculations allow to propose a quite different interpretation of the precipitation reaction in Ni-H system in comparison with that available in the literature. In fact, just after installation of the H-saturated sample into the holder and the first stage of hydrogen degassing (see Figure 7), the diffraction pattern contains peak γ_1 , of which position coincides with that of a

pure nickel, and peaks $(111)\gamma_a$ and $(111)\gamma_b$ belonging to the ordinary H solid solution. After subsequent series of hydrogen degassing, diffraction patterns reveal the coexistence of two hydrogen solid solutions in nickel, γ_1 and γ_2 .

The hydrogen degassing is accompanied by the change in their fractions, whereas their hydrogen concentrations remain unchanged. In other words, the figurative point in the Ni-H phase diagram shifts in the course of hydrogen degassing along the conode towards the decreased total hydrogen content within the crown which borders the T-C area of miscibility gap. Let us compare the proposed interpretation with the features of the phase diagrams for Ni-H system obtained in [10-13], which is presented in Figure 1. The T-P diagram is based on the hydrogen dissolution in nickel under high gaseous hydrogen pressures up to 20 kbar with subsequent cooling to low temperatures and measurements of electroresistivity [10, 11]. The T-C diagram, see insert in Figure 1, is obtained using X-rays of synchrotron radiation for measurements at high hydrogen gaseous pressures during heating and cooling at 1.1 to 5.4 GPa [12, 13].

The diagram from [10, 11] contains the phase γ_1 with the low hydrogen content, the “nickel hydride” γ_2 with high hydrogen content and the intermediate area where the γ_1 to γ_2 transition proceeds. As already noted in the Introduction, the following remarks can be made in relation to the author’s interpretation of their T-P diagram: (i) the nickel hydride exists in a broad area of hydrogen contents, whereas chemical compounds are expected to have a stoichiometric composition or the solid solution can be formed with some deviations from stoichiometry within the narrow concentration range; (ii) with increasing temperature, the intermediate area is narrowing and the border curves γ_2 and γ_1 are intersecting each other, which is a sign for the crown in the phase diagram; (iii) if so, what a phase is thermodynamically stable at temperatures above 400 °C: γ_1 or γ_2 ?

The diagram obtained in [12, 13] clearly shows the crown of miscibility gap with the consolute temperature T_c of 360 °C, whereas the H solid solution exists within the whole measured concentration range above T_c . It is relevant to note that a similar phase diagram is found for the Pd-H system and its interpretation is also proposed in terms of “Pd hydride”, see e.g. [39-41]. The β -phase, i.e. Pd hydride, is claimed to exist within the frame of high hydrogen contents, whereas the α -phase, or α -hydride, with the same crystal lattice is observed at low hydrogen contents, and the both phases coexist within the crown with the consolute temperature T_c of about 300 °C. Above T_c , the α - and β -phases coexist without any phase borders in the phase diagram, like it occurs in the T-P Ni-H diagram.

The interesting results were obtained when the saturation of palladium with hydrogen was carried out at temperatures below or above T_c [40, 41]: (i) a strong hardening and surface relief due to the intersection of the 2-phase region at temperatures below T_c , (ii) the absence of hardening and surface relief above T_c . Clearly, this effect occurs due to difference in the specific volumes of the two solid solution within the area of miscibility gap and is absent if the hydrogen concentration increases within the area of a homogeneous solid solution.

- ***Metal hydrides and thermodynamics.***

Let us finally analyze the data about metal hydrides formed under high hydrogen pressures in a number of d-metals, e.g., Cr, Mn, Fe, Co, Ni, Mo, Tc, Rh, Pd, Re, see e.g. [42-45]. All these hydrides have been shown to exist within a wide range of hydrogen contents. In case of Co, Ni, Rh, Pd, they have the crystal lattices identical with those of parent metals, which suggests that, in fact, they are just oversaturated solid solutions. In contrast, the hydrides in systems Ti-H and Zr-H have definite stoichiometric chemical compositions. Their crystal lattices are different from those of parent metals, which corresponds to the first type of the Gibbs' precipitation reactions, where an oversaturated solid solution and a precipitate are described by the quite different curves of free energy versus concentration.

In case of Cr, Mn, Fe and Mo, the hydrogen-induced $\gamma \rightarrow \epsilon$ transformation proceeds. The "ε-hydrides" with the hcp crystal lattice exist in the wide concentration range, which is also a sign of the solid solutions, not of the chemical compounds. It is relevant in this relation to refer to the Fe-N phase diagram, see e.g. [33]. In many aspects, nitrogen and hydrogen are similar in their effect on the crystal structure, phase transformations and properties. The both elements increase the density of electron states at the Fermi level [46] and, correspondingly, increase the concentration of free electrons [47, 48], cause the $\gamma \rightarrow \epsilon$ transformation [49] and affect iron properties in a similar way [50, 51].

Like hydrogen, nitrogen is a volatile element, and both are negligibly dissolved of the iron. Like the Fe-H phase diagram, the Fe-N one is constituted not for $p_{N_2} = 1$ bar, but for very high partial pressures of nitrogen provided by the dissociation of ammonia. In fact, it is a projection of various equilibrium states in the temperature-pressure-concentration diagram onto the temperature-concentration plane. The solid solution of nitrogen in the hcp ε-iron is found within the broad range of nitrogen contents starting from 25.8 at.%. It reveals a long-range atomic ordering resulting in the superstructure Fe₂N at 33 at.% with small deviations from the stoichiometry within the narrow concentration range. This superstructure is conventionally denoted as ζ-nitride. However, so far, no attempts have been undertaken to apply term "nitride" to the whole concentration range of the hcp Fe-N solid solution.

Therefore, there are no convincing arguments to denote as hydrides the oversaturated hydrogen solid solutions obtained artificially under high hydrogen pressures and having no inherent signs of the chemical compounds.

Summary

The study of the Ni-H system by means of *ab initio* atomic calculations has been carried out. It is shown that the total cohesion energy of the calculated structure monotonically decreases with increasing hydrogen concentration, which suggests that the precipitation reaction in this system occurs without any energy barrier. This result and the identity of the crystal lattices of the parent metal and the precipitate indicate that the free energy-concentration dependence of both phases is described by a single curve in accordance with the Gibb's second type of precipitation reaction in the oversaturated solid solutions. Moreover, the second derivative of the solution enthalpy has a negative sign within the range of the hydrogen concentrations of 0.03 to 0.75. Such a behavior gives evidence for decomposition of solid solution within the concentration range via spinodal mechanism. This result is confirmed by the obtained X-ray diffraction data and consistent

with those available in the literature. The results of calculations of hydrogen effect on the density of electron states at the Fermi level are consistent with the existing data about the correlation between the second derivative of the solution enthalpy and the density of states at the Fermi level in case of decomposition of solid solutions via spinodal mechanism.

The analysis of a number studies of “metal hydrides” apparently obtained under high gaseous hydrogen pressures leads to the conclusion that, in their majority, the formation of oversaturated solid solutions or the $\gamma \rightarrow \epsilon$ phase transformation between two solid solutions occurs.

References

- [1] Baranowski B, Szklarska-Smialowska Z, Smialowski M. Kinetics of H desorption from Ni at 20°C. Bull Acad Pol Sci 1958;6:179.
- [2] Baranowski B. The kinetics of saturation of electrolytic nickel layers with cathodic hydrogen. Bull Acad Polon Sci 1959;7:907.
- [3] Janko A. X-ray studies of nickel charged electrolytically with hydrogen. Bull Acad Polon Sci 1960;8:131.
- [4] Cable JW, Wollan EO and Koehler WC. The crystal structure of nickel hydride. J de Physique 1964;25:460.
- [5] Baranowski B, Filipek SM. 45 Years of nickel hydride—History and perspectives. J Alloys Compd 2005;404-406:2-6.
- [6] Baranowski B and Szklarska-Smialowska Z. A galvanostatic and potentiostatic study of the nickel-hydrogen system. Electrochim Acta 1964;9:1497.
- [7] Juskenas R, Selskis A and Kadziauskiene V. *In situ* X-ray diffraction investigation of nickel hydride formation during cathodic charging of Ni. Electrochim Acta 1998;43:1903-1011.
- [8] Rashkov S, Monev M and Tomov I. Electrochemical formation and disintegration of the Ni-H phase in bright nickel coatings. Surf Technol 1982;16:203.
- [9] Tomov I, Monev M, Mikhailov M and Rashkov S. X-ray diffraction study of anisotropy by the formation and decomposition of nickel hydride. Part II: Decomposition kinetics. J Appl Electrochem 1992;22:82.
- [10] Ponyatovsky EG, Antonov VE, Belash IT. Phase T-P diagram of Ni-H system at temperatures up to 630 K and pressures up to 18 kbar (in Russian). Reports of USSR Academy of Sciences 1976;229:391-393.
- [11] Antonov VE, Belash IT, Ponyatovsky EG. Phase T-P diagrams in N-D and Ni-H systems at temperatures up to 375 °C and pressures up to 20 kbar (in Russian). Reports of USSR Academy of Sciences 1977;233:1114-1117.
- [12] Shizuku Y, Yamamoto S, Fukai Y. Phase diagram of the Ni-H system at high hydrogen pressures. J Alloys Compd 2002;336:159-162.
- [13] Fukai Y, Yamatomo S, Harada S, Kanazawa M. The phase diagram of the Ni-H system revisited. J Alloys Compd 2004;372:L4-L5.
- [14] Hohenberg P and Kohn W. Inhomogeneous electron gas. Phys Rev B 1964;136:864.

- [15] Kohn W and Sham LJ. Self-consistent equations including exchange and correlation effects. *Phys Rev A* 1965;140:1133.
- [16] Blaha P, Schwarz K, Madsen GKH, Kvasnicka D and Luitz J. WIEN2k, An Augmented Plane Wave + Local Orbitals Program for Calculating Crystal Properties. Karlheinz Schwarz, Techn. Universitat Wien, Austria (2001).
- [17] Perdew JP, Burke S and Ernzerhoff M. General gradient approximation made simple. *Phys Rev Lett* 1996;77:3865.
- [18] Monkhorst HJ and Pack JD. Special points for Brillouin-zone integrations. *Phys Rev B* 1976;13:5188.
- [19] Murnaghan FD. The compressibility of media under extreme pressures. *Proc Natl Acad Sci* 1944;30:244.
- [20] Huber KP and Hertzberg G. *Molecular Spectra and Molecular Structure IV: Constants of Diatomic Molecules*. Van Norstrand Reinhold (ed.), New York, 1979.
- [21] Parlinski K. *Software Phonon*, Cracow, 2010.
- [22] Parlinski K, Li ZQ and Kawazoe Y. First-principles determination of the soft mode in cubic ZrO₂. *Phys Rev Lett* 1997;78:4063.
- [23] Kunc K and Martin RM. Ab initio force constants of GaAs: A new approach to calculation of phonons and dielectric properties. *Phys Rev Lett* 1982;48:406.
- [24] Yin MT and Cohen ML. Theory of lattice-dynamical properties of solids: Application to Si and Ge. *Phys Rev B* 1982;26:3259.
- [25] Wollan EO, Cable JW and Koehler WC. The hydrogen positions in face centered cubic nickel hydride. *J Phys Chem Solids* 1963;24:1141.
- [26] Papastaikoudis C, Lengeler B and Jager W. Electrical resistivity of hydrogen in nickel. *J Phys F: Met Phys* 1983;13:2257.
- [27] Robertson WR. Hydrogen permeation, diffusion and solution in nickel. *Z Metallkd* 1973;64:436.
- [28] Yamakawa K and Fujita FE. Diffusion of hydrogen in hydrogen-quenched nickel. *Jpn J Appl Phys* 1977;16:1747.
- [29] Zeng K, Klassen T, Oelerich W and Bormann R. Thermodynamics of the Ni-H system. *J Alloys Compd* 1999;283:151.
- [30] Bauer HJ and Schmidbauer E. Über den Einfluß elektrolytisch abgeschiedenen Wasserstoffs auf die Magnetisierung von Nickel. *Z Phys* 1961;164:367.
- [31] Baranowski B, Majchrzak S, Flanagan TB. The volume increase of fcc metals and alloys due to interstitial hydrogen over a wide range of hydrogen contents *J Phys F: Metal Physics* 1971;1:258.
- [32] Doherty RD, *Diffusive Phase Transformations in the Solid State* (Eds. Cahn RW and Haasen P) (Physical Metallurgy: Elsevier Science BV: 1996), Ch. 15, p. 1369.
- [33] Hansen M, Anderko K. *Constitution of Binary Alloys*. McGraw-Hill Inc, New York –Toronto – London. 1958, pp. 670-675.
- [34] San Marchi C, Somerday BP and Robinson SL. Permeability, solubility and diffusivity of hydrogen isotopes in stainless steels at high gas pressures. *Int J Hydrogen Energy* 2007;32:100.

- [35] Jones H. Concentrated solid solutions of normal metals. *J Phys Radium* 1962;23:637.
- [36] Olsson P, Abrikosov IA and Wallenius J. Electronic origin of the anomalous stability of Fe-rich bcc Fe-Cr alloys. *Phys Rev B* 2006;73:104416.
- [37] Alling B, Karimi A and Abrikosov IA. Electronic origin of the isostructural decompositions in cubic $M_{1-x}Al_xN$ ($M=Ti, Cr, Sc, Hf$): A first-principles study. *Surf Coat Tech* 2008;203:883.
- [38] Smirnova EA, Korzhavyi PA, Vekilov YuKh, Johansson B and Abrikosov IA. *Phys Rev B* 2001;64:020101(R).
- [39] Maeland G, Gibb TRP. X-ray diffraction observation of the Pd-H₂ system through the critical region. *J Phys Chem* 1961;165:1270-1273.
- [40] Goltsova MV, Artemenko YuA, Zhiron GI, Zaitsev VI. Video-investigation of reverse hydride transformations in the Pd-H system. *Intern J Hydrogen Energy* 2002;27:757-776.
- [41] Zhiron GI, Goltsov VA, Shatalov GE, Glyakov DA. Mechanical properties and fine structure of annealed and hydrogen-phase-hardened palladium (in Russian). *Fizika metallov metallovedenie* 2006;101:103-112.
- [42] Somenkov VA, Glazkov VP, Irodova AV, Shilstein S. Crystal structure and volume effects in the hydrides of d metals. *J Less-Common Metals* 1987;1129:171-180.
- [43] Ponyatovsky EG, Belash IT. Formation and decomposition of chromium hydride at temperatures up to 400 °C and pressures up to 20 kbar (in Russian). *Reports of USSR Academy of Sciences* 1976;229:1171-1173.
- [44] Antonov VE. Phase transformations, crystal and magnetic structures of high pressure hydrides of d-metals. *J Alloys Compd* 2002;330-332:110-116.
- [45] Antonov VE, Baier M, Dorner B, Fedorov VK, Grosse G, Kolesnikov AI, Ponyatovsky EG, Schneider G, Wagner FE. High-pressure hydrides of iron and its alloys. *J Phys Condensed Matter* 2002;14:6427-6445.
- [46] Gavriljuk VG, Shanina BD, Syvanyuk VN, Teus SM. Electronic effect on hydrogen brittleness of austenitic steels. *J Appl Phys* 2010;108:083723 (1-9).
- [47] Shanina BD, Gavriljuk VG, Konchits AA, Kolesnik SP, Tarasenko AV. Exchange interaction between electron subsystems in iron-based F.C.C. alloys doped by nitrogen or carbon. *Phys Stat Sol (a)* 1995;149:711-722.
- [48] Shanina BD, Gavriljuk VG, Kolesnik SP, Shvanyuk VN. Paramagnetic spin resonance in hydrogen-charged stainless austenitic steels. *J Phys D: Appl Phys* 1999;32:298-304.
- [49] Teus SM, Shvanyuk VN, Gavriljuk VG. Hydrogen-induced $\gamma \rightarrow \epsilon$ transformation and the role of ϵ -martensite in hydrogen embrittlement of austenitic steels. *Mat Sci & Eng A* 2008;497:290-294.
- [50]. Gavriljuk VG, Shanina BD, Syvanyuk VN. Hydrogen embrittlement of austenitic steels: electron approach. *Corros Reviews* 2013;31:33-50.
- [51] V. G. Gavriljuk. Carbon, Nitrogen, and Hydrogen in Iron-Based Solid Solutions: Similarities and Differences in Their Effect on Structure and Properties. *Metallofiz. Noveishie Tekhnol* 2016;38:67-98. DOI: 10.15407/mfint.38.01.0067.